



1 Analysis of European ozone trends in the period 1995–2014

2 Yingying Yan^{1,2}, Andrea Pozzer¹, Narendra Ojha¹, Jintai Lin³, Jos Lelieveld¹

3 ¹ Atmospheric Chemistry Department, Max Planck Institute for Chemistry, Mainz, Germany

4 ² Department of Atmospheric Science, China University of Geosciences, Wuhan, China

5 ³ Laboratory for Climate and Ocean-Atmosphere Studies, Department of Atmospheric and
6 Oceanic Sciences, School of Physics, Peking University, Beijing 100871, China

7 Email: andrea.pozzer@mpic.de

8 Abstract

9 Surface-based measurements from the EMEP network are used to estimate the changes in surface
10 ozone levels during the 1995–2014 period over Europe. It is shown that a significantly decreasing
11 trend in the 95th percentile ozone concentrations has occurred, especially during noontime (0.9
12 $\mu\text{g}/\text{m}^3/\text{y}$), while the 5th percentile ozone concentrations continued to increase with a trend of 0.3
13 $\mu\text{g}/\text{m}^3/\text{y}$ during the study period. With the help of numerical simulations performed with the
14 global chemistry-climate model EMAC, the importance of anthropogenic emissions changes in
15 determining these changes are investigated. The EMAC model is found to successfully capture
16 the observed temporal variability in mean ozone concentrations, as well as the contrast in the
17 trends of 95th and 5th percentile ozone over Europe. Sensitivity simulations and statistical analysis
18 show that a decrease in European anthropogenic emissions had contrasting effects on surface
19 ozone trends between the 95th and 5th percentile levels, and that background ozone levels have
20 been influenced by hemispheric transport, while climate variability generally regulated the inter-
21 annual variations of surface ozone in Europe.

22 1. Introduction

23 Tropospheric ozone has detrimental effects on human health, and elevated concentrations at the
24 surface are of concern over most of the European region (Hjellbrekke and Solberg, 2002; WHO,
25 2013; EEA, 2013; Lelieveld et al., 2015). The European Union (EU) Air Quality Directive sets
26 four standards for surface ozone to reduce its impacts on human health and crop yields
27 (<http://eur-lex.europa.eu/legal-content/EN/TXT/HTML/?uri=CELEX:32008L0050&from=EN>).

28 The standards are: information threshold, (1-hour average: 180 $\mu\text{g}/\text{m}^3$), alert threshold (1-hour
29 average: 240 $\mu\text{g}/\text{m}^3$), long-term objective (maximum diurnal 8-hour mean: 120 $\mu\text{g}/\text{m}^3$), and the
30 target value (long-term objective should not be exceeded more than 25 days per year, averaged
31 over 3 years). Exceedances are particularly frequent in regions close to high ozone precursor
32 emissions during summer with stagnant meteorological conditions, associated with persistent
33 high temperatures. Since a substantial decrease in precursor concentrations has been achieved in
34 Europe in recent decades, the number of exceedances has declined (Guerreiro et al., 2014), in line



35 with a long-term downward trend of pollution emissions (Colette et al., 2011; Wilson et al., 2012).
36 Further, a number of studies have shown that European ozone levels are on average decreasing in
37 the last 20 years (as example, Jonson et al., 2010). Nevertheless, background ozone changes over
38 Europe are not so clear (Wilson et al., 2012), being sensitive to climate conditions and
39 intercontinental transport of O₃ and its precursors, and are significant in view of tropospheric
40 chemistry (Lelieveld and Dentener, 2000).

41 The response of surface ozone to a changing climate, with potentially more frequent heat
42 extremes (Bloomer et al., 2009; Jacob and Winner, 2009; Cooper et al., 2012; Fu et al., 2015; Lin
43 et al., 2015; Simon et al., 2015), and concurrent changes in anthropogenic emissions of precursor
44 gases (Bloomer et al., 2009; Fu et al., 2015; Strode et al., 2015; Yan et al., 2017) may pose a
45 challenge for air quality management. Observation and model-based analyses of ozone trends in
46 responses to climate change (Bloomer et al., 2009), precursor emissions (Bloomer et al., 2009;
47 Lefohn et al., 2010), and long-range transport (Lin et al., 2015) have been conducted for North
48 America (Strode et al., 2015; Lin et al., 2017; Yan et al., 2017), several Asian regions (Brown-
49 Steiner et al., 2015; Lin et al., 2017) and also for Europe (Meleux et al., 2007, Wilson et al., 2012,
50 Jonson et al., 2006). For Europe, the connection between climate and ozone levels has been
51 subject of large number of studies, notably to investigate the effects of climate change on surface
52 ozone levels (Langner et al., 2005; Meleux et al., 2007; Colette et al., 2011; Langner et al., 2012.)

53 Tropospheric ozone is produced photochemically during daytime, mainly from the photolysis of
54 nitrogen dioxide (NO₂), while NO₂ levels are strongly influenced by radicals and their precursors,
55 including organic compounds. Due to the complex photo-chemistry involved, the amount of
56 ozone formed responds nonlinearly to changes in precursor emissions and is sensitive to
57 variations in air temperature, radiation and other climatic factors (Fu et al., 2015; Monks et al.,
58 2015; Coates et al., 2016). Ozone can be destroyed via reactions with NO_x (i.e., ozone titration)
59 especially during nighttime, and thus a reduction in NO_x emissions could result in more ozone
60 (Jhun et al., 2014; Yan et al., 2017). Previous studies of European ozone have focused on daytime
61 or diurnal mean ozone with little attention paid to the daytime-nighttime contrast in ozone
62 changes (Colette et al., 2011; Wilson et al., 2012; Guerreiro et al., 2014).

63 Our work contrasts the trends of the monthly 5th and 95th percentile European ozone levels at
64 hourly levels over the period 1995–2014, based on the hourly ozone measurements from the
65 EMEP network. Additionally, numerical simulations from the global chemistry-climate model
66 ECHAM5/MESSy (EMAC) are conducted to evaluate the model's ability in capturing ozone
67 trends over Europe and to investigate the underlying importance of the meteorology and emission
68 changes for the observed ozone trends.

69 The manuscript is organized as follows: the observational dataset, model simulations and analysis
70 methods are described in Section 2. In Section 3, the average linear trends for the European
71 domain are estimated and analyzed separately for the monthly, seasonal and annual surface 5th,
72 50th, and 95th percentiles of the observed ozone concentrations. We then compare the observed



73 ozone trends and variability to results of the atmospheric chemistry – general circulation model
74 EMAC. To investigate the effects of anthropogenic emissions and climate variability on observed
75 European ozone changes, we conduct a sensitivity simulation with constant emissions and
76 statistical analysis with the ERA-Interim 2-meter temperature data in Section 4. Followed by the
77 conclusions in Section 5.

78 2. Methods and Data

79 2.1 Ozone measurements

80 The hourly ground-level ozone measurements over 1995–2014 have been obtained from the
81 Chemical Coordination Centre of *European Monitoring and Evaluation Programme* (EMEP)
82 network (<http://www.nilu.no/projects/ccc/emepdata.html>). Table 1 shows the number of
83 measurement sites (varies from 113 to 137) and the percentage of missing hourly data in each
84 year. Fig. 1 further shows the site distribution. Since many of the stations are not operating
85 continuously during the study period (Fig. 1), we have included only those sites in the analysis
86 which fulfill the criteria defined by Cooper et al. (2012). Such data selection criteria are further
87 applied for the US ozone trends analysis with the EPA-AQS measurements by Yan et al. (2017).
88 First, we discard the observational days with the valid hourly data less than 66.7% in any daytime
89 or nighttime. Then, we discard the particular season with less than 60 days containing valid data
90 in any season. Finally, for any season, we keep the data with valid seasonal mean ozone more
91 than 15 years during 1995–2014; otherwise we discard the data in all years for the particular
92 season. Fig. 1 shows the final selected 93 sites satisfying above criteria for the analysis.

93 We calculated the linear trends for the European surface ozone at individual hours, and mean
94 values for daytime (local time: 07:00–19:00), nighttime (local time: 19:00–07:00) and full days
95 (24 h). For each daytime or nighttime period, the missing data varies between 6.8 and 34.6%
96 (Table 1). The monthly 5th, 50th and 95th percentile ozone concentrations for each period (per
97 hour, daytime, nighttime and diurnal) are derived from the lowest, middle and highest 5th
98 percentile hourly ozone mixing ratios of the corresponding period in each month.

99 To calculate the ozone trends per hour, during daytime, nighttime and per day, we then use the
100 following statistical trend model (Weatherhead et al., 1998; Yoon and Pozzer, 2014):

$$101 Y_t = \mu + S_t + \omega X_t + N_t$$

102 Where Y_t denotes the monthly time series of ozone, μ is a constant term representing the offset,
103 $X_t = t/12$ (with t as month) the number of years in the timeseries, and ω is the magnitude of the
104 trend per year. S_t is a seasonal component in the trend estimates. N_t is the residual term of the
105 interpolation. As the seasonal component does not have much impact on the statistical properties
106 of the estimates of the other terms in the model, we use the deseasonalized monthly data to
107 perform the trend analysis with a model of the form:



$$Y_t = \mu + \omega X_t + N_t$$

108 Using this formulation the linear trends are also analyzed separately for the observed monthly,
109 seasonal and annual surface ozone concentration. The 5th, 50th and 95th percentile ozone
110 concentrations are derived from the lowest, middle and highest 5th percentile of the full set of
111 measurements (i.e., hourly ozone mixing ratios) of the corresponding period.

112 The standard deviation of ozone trends over the European stations is calculated with:

$$113 \quad \sigma = \sqrt{\frac{1}{N} \sum_{i=1}^N (\omega_i - \alpha)^2}$$

114 where N is the total number of sites, ω_i is ozone trend at individual sites and α represents the
115 average ozone trend.

116 **2.2 ERA-Interim 2-meter temperature data**

117 The 2-meter temperature data is from the reanalysis product ERA-Interim, provided by the
118 European Centre for Medium Range Weather Forecast (ECMWF) Public Datasets web interface
119 (<http://apps.ecmwf.int/datasets/>), covering the data-rich period from 1979 and continuing in real
120 time (Dee et al., 2011). Compared to the ERA-40, the ERA-Interim has an improved
121 representation of the hydrological cycle, and stratospheric circulation (Dee and Uppala, 2009;
122 Dee et al., 2011). The ERA-Interim atmospheric model and reanalysis system uses cycle 31r2 of
123 ECMWF's Integrated Forecast System (IFS), configured for 60 vertical levels up to 0.1 hPa. The
124 horizontal-spatial resolution is either in a full T255 spectral resolution or in the corresponding
125 N128 reduced Gaussian grid (Dee et al., 2011). ERA-Interim assimilates four analyses per day, at
126 00, 06, 12 and 18 UTC. ECMWF public website provides a large variety of data in uniform
127 lat/long grids varying from 0.125° to 3°. Out of those, here, we analyze the monthly mean 2-
128 meter temperature data which are archived on the 0.75° latitude by 0.75° longitude grid.
129 Additional information (e.g. on current data availability) is available on the ECMWF website at
130 <http://www.ecmwf.int/research/era>.

131 **2.3 Atmospheric chemistry modeling**

132 The ECHAM5/MESSy Atmospheric Chemistry (EMAC) model has been used to simulate
133 surface ozone for the 1995–2014 periods. The EMAC model applies the second version of the
134 Modular Earth Submodel System (MESSy2) to link multi-institutional computer codes (Jockel et
135 al., 2016). The core atmospheric model is the 5th generation European Centre Hamburg general
136 circulation model (ECHAM5) (Roeckner et al., 2006). EMAC simulated gas-phase tracers as well
137 as aerosols have been extensively evaluated in previous studies (e. g. Pozzer et al., 2007; Pozzer
138 et al., 2012).



139 In this work, we use the archived RC1SD-base-10a simulation results from the EMAC model
140 conducted by the ESCiMo project (Jockel et al., 2016). The model results were simulated with
141 version 5.3.02 for ECHAM5 and version 2.51 for MESSy. The archived data were obtained with
142 a T42L90MA spatial resolution, i.e., with a T42 spherical representation which is corresponding
143 to a quadratic Gaussian grid with approximately 2.8 latitude by 2.8 longitude, and 90 levels in the
144 vertical, with the top level up to 0.01 hPa. To reproduce the observed meteorology, the method of
145 Newtonian relaxation towards ERA-Interim reanalysis data (Dee et al., 2011) is applied to
146 weakly nudge the dynamics of the general circulation model. Differently from the work of Jöckel
147 et al. (2016), the model was re-run to cover the full period of measurements and also with a 1-
148 hourly temporal resolution for ozone, in order to compare model results with hourly
149 observational data. We also conducted a sensitivity simulation in which the anthropogenic
150 emissions were kept constant throughout the years to investigate the effects of emissions on
151 ozone trends.

152 Anthropogenic emissions in the model are incorporated as prescribed sources following the
153 Chemistry-Climate Model Initiative (CCMI) recommendations (Eyring et al., 2013), using the
154 MACCity (Monitoring Atmospheric Composition & Climate/City Zero Energy) emission
155 inventory, which includes a seasonal cycle (monthly resolved). Additionally, the emissions are
156 vertically distributed as described by Pozzer et al. (2009). Since the total NMVOCs (non-methane
157 volatile organic compounds) values for anthropogenic sectors are not provided by the MACCity
158 raw dataset, they are recalculated from the corresponding species (Jockel et al., 2016).

159 Emissions from natural sources have been prescribed as well, either as monthly resolved or
160 annually constant climatology. The spatial and temporal distributions of biogenic NMHCs are
161 based on Global Emissions Initiative (GEIA). Further details of the model setup on the emissions,
162 physical and chemical processes as well as the model evaluation with observations can be found
163 in Jöckel et al. (2016).

164 **3. Results**

165 **3.1 Ozone trends in EMEP measurements**

166 Fig. 2 shows the trends in ozone concentrations (monthly mean, 5th, 50th and 95th percentile) over
167 Europe during the 1995-2014 period, for each hour of the day. While the average ozone
168 concentrations (and 50th percentiles) do not show significant trends, the 5th and 95th percentile
169 ozone show significant trends with a clear diel cycle. The 95th percentile ozone shows a
170 decreasing trend over Europe during the 1995-2014 period with the trend being most pronounced
171 ($-0.9 \pm 0.5 \mu\text{g}/\text{m}^3/\text{y}$) during midday (1100-1500 h). 95th percentile ozone concentrations also
172 show a decreasing trend during the night, however the trends are observed to be smaller ($-0.5 \pm$
173 $0.35 \mu\text{g}/\text{m}^3/\text{y}$). Here the standard deviation depicts the variability of the trends among the stations,
174 and therefore reflects the almost homogeneous decrease over entire Europe. Interestingly, in
175 contrast with the 95th percentile, the 5th percentile ozone over Europe shows an increasing trend



176 especially during midday ($0.3 \pm 0.16 \mu\text{g}/\text{m}^3/\text{y}$). Further, the temporal evolutions of ozone
177 anomalies during the 1995–2014 period are shown for 5th and 95th percentile in Fig. S1. The 95th
178 percentile ozone trend indicates a general decline in the photochemical buildup of ozone during
179 noon hours, with the exception of strongly enhanced ozone during 2003. The inter-annual
180 variability is observed to be very large with ozone anomalies in excess of $35 \mu\text{g}/\text{m}^3$ in 2003
181 relative to 2014. For 95th percentile ozone, the sharp increase by up to $20 \mu\text{g}/\text{m}^3$ in the year 2003
182 occurred during a strong European heat wave (Section 4.2). The analysis of individual year
183 observations here shows that the increasing trend in the 5th percentile ozone is a robust feature
184 with most of the recent years showing stronger noontime build up in ozone as compared to the
185 1990s. During the study period the variability in noontime ozone anomalies is however lower
186 ($\sim 10 \mu\text{g}/\text{m}^3$) in the 5th percentile ozone compared to the 95th percentile ozone.

187 Consistently with the results obtained for hourly ozone, when the observational data is reduced to
188 diurnal values, a growth rate of $0.22 \pm 0.15 \mu\text{g}/\text{m}^3/\text{y}$ is calculated for the 5th percentile ozone,
189 while a stronger decline rate of $-0.57 \pm 0.34 \mu\text{g}/\text{m}^3/\text{y}$ is estimated for the 95th percentile ozone
190 (see Table 2). Hereafter we will mainly focus on trends in the daytime mean, nighttime mean, 5th
191 percentile and 95th percentile ozone concentrations.

192 The observed long-term reduction in 95th percentile ozone concentrations over Europe concurs
193 with the reduction in anthropogenic emissions of ozone precursors. Anthropogenic emissions of
194 NO_x and CO over Europe declined by 35% and 58%, respectively, as calculated from the
195 MACCity inventory. Slower rates of ozone reduction during nighttime are suggested to be
196 combined effects of reduced titration due to lower NO_x emissions, and an increase in the global
197 background ozone concentrations during this period, probably due to growing precursor
198 emissions in China since 1995, which has been predicted by Lelieveld and Dentener (2000) based
199 on atmospheric chemistry – transport modeling, and corroborated by satellite observations
200 (Richter et al., 2005; Krotov et al., 2016). The effect of anthropogenic emissions is discussed in
201 more detail in the Section 4.1.

202 Fig. 3 further shows ozone trends for each month of the year. The slight growth rates in the 5th
203 percentile ozone are approximately equally distributed at the level of $0.1 \pm 0.12 \mu\text{g}/\text{m}^3/\text{y}$.
204 Conversely, the monthly trends for the 95th percentile ozone are negative with a most rapid
205 decrease rate of $-1.67 \pm 0.4 \mu\text{g}/\text{m}^3/\text{y}$ in August. For the 50th percentiles (mean) the seasonal cycle
206 of ozone trends decline unevenly from January to August, then pick up in the following months.
207 It leads to the fastest ozone growth in December when the ozone production is minor due to the
208 relatively lowest solar UV fluxes and temperatures, and the maximum ozone decline in August,
209 which is the photochemically most active month in Europe. In December, the 50th (mean)
210 percentile ozone increases at a rate of $0.41 \pm 0.21 \mu\text{g}/\text{m}^3/\text{y}$ ($0.32 \pm 0.09 \mu\text{g}/\text{m}^3/\text{y}$), while a decline
211 rate of $-0.40 \pm 0.24 \mu\text{g}/\text{m}^3/\text{y}$ ($-0.51 \pm 0.13 \mu\text{g}/\text{m}^3/\text{y}$) is calculated in August.



212 Table 3 shows the trends in seasonal ozone concentrations over Europe analyzed separately for
213 day- and nighttime. The ozone concentrations show pronounced differences in trends over the
214 different seasons. The mean surface ozone in summer, averaged over the selected 93 sites,
215 declines at rates of $-0.32 \pm 0.24 \mu\text{g}/\text{m}^3/\text{y}$ and $-0.20 \pm 0.27 \mu\text{g}/\text{m}^3/\text{y}$ during day- and nighttime,
216 respectively. It is mainly related to the rapid decline in the highest levels (95th percentile) of
217 ozone with rates of $-1.10 \pm 0.61 \mu\text{g}/\text{m}^3/\text{y}$ (daytime) and $-0.71 \pm 0.52 \mu\text{g}/\text{m}^3/\text{y}$ (nighttime).
218 Although the 95th percentile ozone in spring declines almost as fast as during summer, the
219 decrease in spring for the 95th percentile ozone is compensated by the growth in 5th percentile
220 ozone, leading to much lower decrease rates in spring compared to summer for the mean ozone
221 concentrations. Finally, in winter ozone grows at a rate of $\sim 0.10 \mu\text{g}/\text{m}^3/\text{y}$. This increase occurs
222 mostly in the lower level (5th percentile) ozone concentrations, with growth rates of 0.25 ± 0.15
223 $\mu\text{g}/\text{m}^3/\text{y}$ (daytime) and $0.14 \pm 0.22 \mu\text{g}/\text{m}^3/\text{y}$ (nighttime).

224 For the trends in annual mean ozone mixing ratios, a decline in the 95th percentile ozone (daytime:
225 $-0.81 \pm 0.46 \mu\text{g}/\text{m}^3/\text{y}$; nighttime: $-0.57 \pm 0.36 \mu\text{g}/\text{m}^3/\text{y}$) is observed while an increase in the 5th
226 percentile ozone (0.22 ± 0.17 and $0.16 \pm 0.17 \mu\text{g}/\text{m}^3/\text{y}$ for day- and nighttime, respectively, is
227 calculated, resulting in statistically not-significant decreasing trends (daytime: -0.09 ± 0.24 ;
228 nighttime: $-0.05 \pm 0.23 \mu\text{g}/\text{m}^3/\text{y}$) (Table 3).

229 Fig. 4 further shows the ozone trends distribution site-by-site over the 93 selected stations for
230 daytime mean, 5th and 95th percentile ozone during the four seasons. The 95th percentile ozone
231 trend shows a decline at most of the selected sites, although ozone increases are also visible at
232 several sites, especially in fall-to-winter. The annual ozone trend averaged over all sites during
233 daytime ($-0.61 \mu\text{g}/\text{m}^3/\text{y}$) is nearly twice that during nighttime ($-0.34 \mu\text{g}/\text{m}^3/\text{y}$, Fig. S2). For the 5th
234 percentile ozone, the annual means have grown over the western and central European sites, in
235 contrast with declines in ozone at other locations over the northern and southern Europe.
236 Averaged across all sites, the 5th percentile ozone has slightly grown during day- as well as
237 nighttime. The regional trend contrast is most significant in summertime with an average
238 decrease rate of $-0.03 \mu\text{g}/\text{m}^3/\text{y}$. The ozone trends spatial distribution in the daytime (Fig. 4) much
239 resembles that of the ozone trends in nighttime (Fig. S2) for the mean, 5th percentile as well as
240 95th percentile ozone.

241 3.2 Ozone exceedance trends

242 Based on the European directive for ozone concentrations limits, we calculate the number of
243 exceedances for the information threshold and long-term objective (Fig. 5). Averaged over the
244 selected 93 sites, the exceedances of the information threshold as well as the long-term objective
245 have declined at rates of -3.2% and -2.5% per year relative to 1995. The decrease accelerated
246 after the year 2003, during which a European heat wave raised summer temperatures by 20 to 30%
247 (in degrees Celsius) compared to the seasonal average over a large part of the continent,
248 extending from northern Spain to the Czech Republic and from Germany to Italy. The variations



249 in the exceedances are inter-annually consistent with the changes in the annual 95th percentile
250 ozone, with a significant correlation coefficient of 0.93 for information threshold exceedances
251 and 0.90 for long-term objective exceedances.

252 3.3 Ozone trends from EMAC simulation

253 The same analysis performed on the observations has been carried out on the EMAC model
254 results, i.e., for the same period covered by the observations. To ensure spatiotemporal
255 consistency with the EMEP data, modeled ozone concentrations are sampled at the times and
256 locations of the measurements. Fig. 6 compares the time series of modeled and observed monthly
257 mean ozone over Europe. Although the model overestimates the measurements with a mean bias
258 of 4.3 $\mu\text{g}/\text{m}^3$ over the 1995–2014 period, the simulation results are highly correlated with
259 observed ozone, with a significant correlation coefficient of 0.91. The high bias may be explained
260 by the coarse grid resolution of 2.8 degrees that was applied, leading to the artificial dispersion of
261 localized NO_x emissions, which optimizes NO_x concentrations over Europe with respect to
262 chemical O_3 formation, also noticed by Joeckel et al (2016). Such overestimation of the observed
263 ozone due to coarse model horizontal resolution has been reported by Lin et al. (2008) and Yan et
264 al. (2014, 2016). The overestimation after 2010 becomes more evident (mean bias 5.4 $\mu\text{g}/\text{m}^3$),
265 mostly due to the emissions used in the model version used, being prescribed up to the year 2005
266 and predicted in the subsequent period. The modeled ozone biases are slightly higher (mean bias:
267 5.2 $\mu\text{g}/\text{m}^3$ and 6.7 $\mu\text{g}/\text{m}^3$ for 1995–2014 and 2010–2014, respectively) compared to the observed
268 de-seasonalized time series. Nevertheless, EMAC model can reproduce the observed inter-annual
269 and seasonal variabilities of ozone, with statistically significant correlation coefficients at most
270 observation sites. For the diurnal, daytime as well as nighttime mean ozone averaged across the
271 93 sites, the model-observation correlation is 0.84–0.92 (0.62–0.70 for de-seasonalized time
272 series).

273 The EMAC modeled ozone trends per hour are shown in Fig. 6. The agreement with the
274 observationally estimated trends is good, although the model tends to overestimate the trends by
275 0.12 $\mu\text{g}/\text{m}^3/\text{y}$, 0.23 $\mu\text{g}/\text{m}^3/\text{y}$, 0.08 $\mu\text{g}/\text{m}^3/\text{y}$, and 0.36 $\mu\text{g}/\text{m}^3/\text{y}$ for the mean, 5th, 50th and 95th
276 percentile ozone, respectively. The measured diurnal cycle of the ozone trends (Fig. 2) is well
277 captured by the EMAC model for the 5th and 95th percentile ozone concentrations. Consistently,
278 the modeled temporal evolutions (Fig. S3) of annual European 5th percentile ozone anomalies are
279 larger compared to the observations ($\sim 15 \mu\text{g}/\text{m}^3$ versus $\sim 10 \mu\text{g}/\text{m}^3$ enhancements during
280 photochemical buildup of ozone at midday hours during 1990–2014), while being smaller for the
281 95th percentile ($\sim 21 \mu\text{g}/\text{m}^3$ versus $\sim 30 \mu\text{g}/\text{m}^3$). Further, the EMAC model reproduces the jump in
282 high level ozone concentrations during the year 2003 that was affected by a major heat wave.

283 For the diurnal mean values, averaged over Europe, the model produces higher growth rates for
284 the 5th percentile ozone and weaker decrease rates for the 95th percentile ozone compared to the
285 observed trends (Table 2). For the 50th percentile and mean ozone trends averaged over Europe,



286 the model shows statistically insignificant changes, similar to the observed trends (Table 2). Fig.
287 S4 further shows the spatial distribution of the simulated diurnal ozone trends. It corroborates that
288 central Europe experiences the highest growth rate for the averaged (also 50th percentile) and 5th
289 percentile ozone concentrations, and the strongest reduction for the 95th percentile ozone during
290 all seasons.

291 For the trends per month, the EMAC model reproduces the observed variability with statistically
292 significant correlation coefficients of 0.88–0.90 for the mean, 50th and 95th percentile ozone
293 trends (Fig. 3 and Fig. S5). Seasonally, for the 95th percentile ozone the modeled ozone trends are
294 much weaker than from measurements in all seasons except the autumn (Table 3). The decreased
295 higher level ozone is probably driven by the anthropogenic ozone precursor emission decline
296 over these years, which has been studied in previous work of ozone change drivers and
297 corroborated in Sect. 3.4 with a sensitivity simulation. For the 5th percentile ozone, especially for
298 the daytime period, the increasing trends are enhanced in the model results during all seasons
299 (Table 3).

300 **4. Anthropogenic emissions and climate variability**

301 **4.1 Effects of anthropogenic emissions**

302 A sensitivity simulation is conducted with constant global anthropogenic emissions to test the
303 sensitivity of observed European ozone to inter-annual variability in climate, by removing the
304 effects of anthropogenic emission changes. Consequently, the decline in European emissions (Fig.
305 S6) is removed from the EMAC model. With constant emissions, the modeled ozone shows a
306 slight increase at the midday hours for the 95th percentile and a slight decrease for the 5th
307 percentile, in contrast to the trends calculated from the control simulation. In the sensitivity
308 simulations no significant trend (less than 0.1 $\mu\text{g}/\text{m}^3/\text{y}$) for any hour of the day is found, and also
309 no contrast in ozone trends between the 5th and 95th percentiles (Fig. 7), which was well
310 reproduced by the control simulation. Therefore, it appears that both the decreases in 95th
311 percentile ozone and the enhancements in 5th percentile ozone are associated with the rapid
312 decline in the precursor gases anthropogenic emissions over Europe, notably of NO_x , prescribed
313 by the MACCity inventory (Fig. S6). These results reflect the effectiveness in controlling high-
314 level ozone, but being unsuccessful in controlling the lower level ozone. Evidently, the 35%
315 reduction in NO_x emissions in Europe was not sufficient to achieve substantial reductions in
316 ozone, especially of background levels, which are affected by growing emissions in Asia that are
317 transported hemispherically (Lelieveld and Dentener, 2000).

318 Averaging over the selected 93 sites, we calculate the number of exceedances for the information
319 threshold both in the control and the sensitivity simulation (Fig. 8). In the control simulation, the
320 exceedances of the information threshold have declined at rates of -2.5% per year relative to 1995,



321 slightly smaller than the observed decrease rate of -3.2%. The variations in exceedances are inter-
322 annually consistent with the observations, with a significant correlation coefficient of 0.61.
323 However, in the sensitivity simulation, the decline rate (-0.6%) in the exceedances is much
324 smaller than the rates in the control simulation and in the observations.

325 By fixing the anthropogenic emissions, ozone trends in each month for the 95th percentile ozone
326 show no obvious decline but rather a slight enhancement with growth rates of -0.23 – 0.50
327 $\mu\text{g}/\text{m}^3/\text{y}$. For the 5th percentile ozone and compared to the control simulation, there is no increase
328 but a slight decrease at a rate of -0.51 – 0.15 $\mu\text{g}/\text{m}^3/\text{y}$ in months of the year (Fig. S7). For the
329 trends in annual mean ozone mixing ratios simulated in the sensitivity simulation, an
330 enhancement in the 95th percentile ozone (daytime: $0.16 \pm 0.18 \mu\text{g}/\text{m}^3/\text{y}$; nighttime: 0.10 ± 0.15
331 $\mu\text{g}/\text{m}^3/\text{y}$) is calculated while a decline in the 5th percentile ozone (-0.11 ± 0.14 and -0.07 ± 0.12
332 $\mu\text{g}/\text{m}^3/\text{y}$ for daytime and nighttime, respectively) is estimated, contrasting to but smaller in the
333 absolute value than the trends in the control simulation. This contrast has been also shown in the
334 trends for individual hour of the day between control and sensitivity simulations (Fig. 7). These
335 results show that the effects of decline in anthropogenic emissions on European ozone change are
336 somewhat offset by the impacts of climate variability. This compensation effect is not only for
337 the high level ozone concentrations, which has been reported by previous studies (Lin et al.,
338 2017), but also for the low level ozone concentrations.

339 **4.2 Effects of heat waves**

340 As discussed in number of studies (e.g., Filleul et al, 2006, Vautard et al, 2005, Garcia-Herrera et
341 al 2010, Vieno et al 2010), the 2003 heat waves caused favorable meteorology for ozone buildup,
342 leading to very high ozone concentrations during the summer period (from July to August). Fig. 9
343 shows the distribution of the difference in the exceedances between 2003 and averaged over
344 1995-2002 for the information threshold as well as the long-term objective over individual site.
345 Except for some northern sites, the exceedances in 2003 are much more frequent than the average
346 from 1995 to 2002 over most of the observational sites, especially over central Europe. This
347 exceedance anomaly distribution in 2003 relative to the period of 1995-2002 coincides with the
348 2-meter temperature anomaly distribution, with a statistically significant correlation up to 0.64
349 (Fig. S8).

350 The exceedance anomaly of information threshold and long-term objective during the year 2003
351 with respect to the 1995-2002 period follows the anomaly in ozone concentrations, in turn
352 consistent with the temperature anomaly. Fig. S9 shows the correlations between the monthly
353 mean 2-meter temperature and the monthly mean, 5th and 95th percentile ozone for diurnal,
354 daytime and nighttime concentrations. It corroborates the high correlations over central Europe
355 with statistically significant values up to ~0.82. Ozone concentrations over the northern sites are
356 negative and insignificantly correlated with temperature. This may be related to the influence of
357 the Northern Atlantic Oscillation, which had an opposite impact on temperature over northern



358 compared to central Europe (Fig. S10). These results underscore that the large-scale climate
359 variability affects the inter-annual variability of European ozone.

360 In the simulation with constant emissions, however, the modeled ozone fluctuation of annual
361 European ozone anomalies for individual hours is comparable in magnitude with the results in the
362 control simulation (Fig. S7). In both simulations, the fluctuation dominates around midday for 5th
363 (~15 $\mu\text{g}/\text{m}^3$ in the base simulation versus ~13 $\mu\text{g}/\text{m}^3$ in sensitivity simulation) and 95th (~21
364 $\mu\text{g}/\text{m}^3$ versus ~20 $\mu\text{g}/\text{m}^3$) percentile ozone (Fig. S7 and Fig. S3). In addition, the variations in the
365 exceedances of the information threshold are inter-annually consistent with the observations and
366 the control simulation, with significant correlation coefficients of 0.54 and 0.56, respectively,
367 comparable to the correlations between observations and control simulation (Fig. 8). Further
368 correlations between the European averaged monthly mean 2-meter temperature and the modeled
369 monthly mean (50th), 5th and 95th percentile ozone in the sensitivity simulation are statistically
370 significant with correlation coefficients of 0.69–0.78 for diurnal, day- and nighttime
371 concentrations, consistent with the correlations (0.70–0.81) between 2-meter temperature and
372 simulated European ozone in the control simulation. These results clearly show that the ozone
373 variations are regulated by climate variations.

374 **5. Conclusions and outlook**

375 Based on EMEP observed ozone in the period 1995–2014, we analyzed the annual and seasonal
376 trends of the mean, the 5th, 50th and 95th percentile of the ozone concentrations at different
377 temporal distributions, i.e., hourly, diurnal, day- and nighttime. Results show that although
378 reductions in anthropogenic emissions have lowered the peak ozone concentrations, especially
379 during daytime in the period 1995–2014, the lower level ozone concentrations have increased
380 continually since 1995 over the 93 sites. This leads to insignificant trends in the 50th percentile
381 and mean ozone. Both the 5th and 95th percentile ozone trends follow a diel cycle with largest
382 trends during periods of strong photochemical activity. These contrasting ozone trends per hour
383 during the day and at different concentration levels are well reproduced by the EMAC chemistry-
384 climate model, although the model slightly overestimates observed ozone at the surface.
385 Furthermore, the numbers of exceedances of the information threshold and long-term objective
386 have continuously declined during the 20-year period considered, and the decrease has
387 accelerated since the year 2003.

388 Sensitivity simulations with constant emissions in the EMAC model, and correlation analysis
389 between modeled ozone and the ERA-Interim 2-meter temperature help distinguish effects of
390 climate and anthropogenic emissions on ozone variations and trends. Climate variability
391 generally regulates the interannual variations of European surface ozone, while the changes in
392 anthropogenic emissions predominantly contribute to ozone trends. However, it appears that the
393 negative ozone trend due to European emission controls has been counteracted by a climate
394 related tendency as well as hemispheric dispersion of pollutants from other regions, notably
395 China..

396 **Acknowledgements**

397 We thank Andries De Vries for discussion. We acknowledge the free use of hourly ozone data
398 from EMEP network (<http://www.nilu.no/projects/ccc/emepdata.html>) and ERA-Interim 2 meter
399 temperature data from the ECMWF.

400 **References**

- 401 Hjellbrekke, A-G., Solberg, S., 2002. Ozone measurements 2000. EMEP/CCC-Report 5/2002.
402 EEA, 2013 EEA, Exposure of Ecosystems to Acidification, Eutrophication and Ozone (Indicator CSI 005), (2013)
403 [http://www.eea.europa.eu/data-and-maps/indicators/exposure-of-ecosystems-to-acidification-2/exposure-of-](http://www.eea.europa.eu/data-and-maps/indicators/exposure-of-ecosystems-to-acidification-2/exposure-of-ecosystems-to-acidification-5)
404 [ecosystems-to-acidification-5](http://www.eea.europa.eu/data-and-maps/indicators/exposure-of-ecosystems-to-acidification-2/exposure-of-ecosystems-to-acidification-5)
405 WHO, 2013 WHO, Review of Evidence on Health Aspects of Air Pollution – REVIHAAP Project, Technical
406 Report World Health Organization, Regional Office for Europe, Copenhagen, Denmark (2013)
407 Eyring, V., Lamarque, J.-F., Hess, P., Arfeuille, F., Bowman, K., Chipperfield, M., Duncan, B., Fiore, A., Gettelman,
408 A., Giorgetta, M., Granier, C., Hegglin, M., Kinnison, D., Kunze, M., Langematz, U., Luo, B., Martin, R.,
409 Matthes, K., Newman, P., Peter, T., Robock, A., Ryerson, A., Saiz-Lopez, A., Salawitch, R., Schultz, M.,
410 Shepherd, T., Shindell, D., St. Helin, J., Tegtmeier, S., Thomason, L., Tilmes, S., Vernier, J.-P., Waugh, D.,
411 and Young, P.: Overview of IGAC/SPARC Chemistry-Climate Model Initiative (CCMI) Community
412 Simulations in Support of Upcoming Ozone and Climate Assessments, available at: [http://www.sparc-](http://www.sparc-climate.org/fileadmin/customer/6_Publications/Newsletter_PDF/40_SPARCnewsletter_Jan2013_web.pdf)
413 [climate.org/fileadmin/customer/6_Publications/Newsletter_PDF/40_SPARCnewsletter_Jan2013_web.pdf](http://www.sparc-climate.org/fileadmin/customer/6_Publications/Newsletter_PDF/40_SPARCnewsletter_Jan2013_web.pdf),
414 2013.
415 Pozzer, A., Jöckel, P., and Van Aardenne, J.: The influence of the vertical distribution of emissions on tropospheric
416 chemistry, *Atmos. Chem. Phys.*, 9, 9417–9432, doi:10.5194/acp-9-9417-2009, 2009.
417 Bloomer, B. J., Stehr, J. W., Piety, C. A., Salawitch, R. J., and Dickerson, R. R.: Observed relationships of ozone air
418 pollution with temperature and emissions, *Geophysical Research Letters*, 36, L09803,
419 10.1029/2009gl0137308, 2009.
420 Brown-Steiner, B., Hess, P. G., and Lin, M. Y.: On the capabilities and limitations of GCM simulations of
421 summertime regional air quality: A diagnostic analysis of ozone and temperature simulations in the US
422 using CESM CAM-Chem, *Atmospheric Environment*, 101, 134-148, 10.1016/j.atmosenv.2014.11.001,
423 2015.
424 Coates, J., Mar, K. A., Ojha, N., and Butler, T. M.: The influence of temperature on ozone production under varying
425 NO_x conditions – a modelling study, *Atmos. Chem. Phys.*, 16, 11601-11615, [https://doi.org/10.5194/acp-16-](https://doi.org/10.5194/acp-16-11601-2016)
426 [11601-2016](https://doi.org/10.5194/acp-16-11601-2016), 2016.
427 Colette, A., Granier, C., Hodnebrog, O., Jakobs, H., Maurizi, A., Nyiri, A., Bessagnet, B., D'Angiola, A., D'Isidoro,
428 M., Gauss, M., Meleux, F., Memmesheimer, M., Mieville, A., Rouil, L., Russo, F., Solberg, S., Stordal, F.,
429 and Tampieri, F.: Air quality trends in Europe over the past decade: a first multi-model assessment,
430 *Atmospheric Chemistry and Physics*, 11, 11657-11678, 10.5194/acp-11-11657-2011, 2011.
431 Cooper, O. R., Gao, R.-S., Tarasick, D., Leblanc, T., and Sweeney, C.: Long-term ozone trends at rural ozone
432 monitoring sites across the United States, 1990-2010, *Journal of Geophysical Research-Atmospheres*, 117,
433 10.1029/2012jd018261, 2012.
434 Dee, D. P., Uppala, S. M., Simmons, A. J., Berrisford, P., Poli, P., Kobayashi, S., Andrae, U., Balmaseda, M. A.,
435 Balsamo, G., Bauer, P., Bechtold, P., Beljaars, A. C. M., van de Berg, L., Bidlot, J., Bormann, N., Delsol,
436 C., Dragani, R., Fuentes, M., Geer, A. J., Haimberger, L., Healy, S. B., Hersbach, H., Holm, E. V., Isaksen,
437 L., Kallberg, P., Köhler, M., Matricardi, M., McNally, A. P., Monge-Sanz, B. M., Morcrette, J. J., Park, B.
438 K., Peubey, C., de Rosnay, P., Tavolato, C., Thepaut, J. N., and Vitart, F.: The ERA-Interim reanalysis:
439 configuration and performance of the data assimilation system, *Quarterly Journal of the Royal*
440 *Meteorological Society*, 137, 553-597, 10.1002/qj.828, 2011.



- 441 Fu, T.-M., Zheng, Y., Paulot, F., Mao, J., and Yantosca, R. M.: Positive but variable sensitivity of August surface
442 ozone to large-scale warming in the southeast United States, *Nature Climate Change*, 5, 454-458,
443 10.1038/nclimate2567, 2015.
- 444 Guerreiro, C. B. B., Foltescu, V., and de Leeuw, F.: Air quality status and trends in Europe, *Atmospheric*
445 *Environment*, 98, 376-384, 10.1016/j.atmosenv.2014.09.017, 2014.
- 446 Jacob, D. J., and Winner, D. A.: Effect of climate change on air quality, *Atmospheric Environment*, 43, 51-63,
447 10.1016/j.atmosenv.2008.09.051, 2009.
- 448 Jhun, I., Coull, B. A., Zanobetti, A., and Koutrakis, P.: The impact of nitrogen oxides concentration decreases on
449 ozone trends in the USA, *Air Quality, Atmosphere & Health*, 1-10, 2014.
- 450 Jockel, P., Tost, H., Pozzer, A., Kunze, M., Kirner, O., Brenninkmeijer, C. A. M., Brinkop, S., Cai, D. S., Dyroff, C.,
451 Eckstein, J., Frank, F., Garny, H., Gottschaldt, K. D., Graf, P., Grewe, V., Kerkweg, A., Kern, B., Matthes,
452 S., Mertens, M., Meul, S., Neumaier, M., Nutz, M., Oberlander-Hayn, S., Ruhnke, R., Runde, T., Sander,
453 R., Scharffe, D., and Zahn, A.: Earth System Chemistry integrated Modelling (ESCiMo) with the Modular
454 Earth Submodel System (MESSy) version 2.51, *Geoscientific Model Development*, 9, 1153-1200,
455 10.5194/gmd-9-1153-2016, 2016.
- 456 Jonson, J. E., Simpson, D., Fagerli, H., and Solberg, S.: Can we explain the trends in European ozone levels?, *Atmos.*
457 *Chem. Phys.*, 6, 51-66, <https://doi.org/10.5194/acp-6-51-2006>, 2006.
- 458 Langner, J., R. Bergström, and V. Foltescu: Impact of climate change on surface ozone and deposition of sulphur and
459 nitrogen in Europe, *Atmospheric Environment*, vol. 39, no. 6, pp. 1129-1141, 2005.
- 460 Langner, J., Engardt, M., Baklanov, A., Christensen, J. H., Gauss, M., Geels, C., Hedegaard, G. B., Nuterman, R.,
461 Simpson, D., Soares, J., Sofiev, M., Wind, P., and Zakey, A.: A multi-model study of impacts of climate
462 change on surface ozone in Europe, *Atmos. Chem. Phys.*, 12, 10423-10440, [https://doi.org/10.5194/acp-12-](https://doi.org/10.5194/acp-12-10423-2012)
463 [10423-2012](https://doi.org/10.5194/acp-12-10423-2012), 2012.
- 464 Lefohn, A. S., Shadwick, D., and Oltmans, S. J.: Characterizing changes in surface ozone levels in metropolitan and
465 rural areas in the United States for 1980-2008 and 1994-2008, *Atmospheric Environment*, 44, 5199-5210,
466 10.1016/j.atmosenv.2010.08.049, 2010.
- 467 Lelieveld, J., and Dentener, F. J.: What controls tropospheric ozone? *J. Geophys. Res.*, 105, 3531-3551, 2000.
- 468 Lelieveld, J., Evans, J. S. F., Ni, M., Giannadaki, D., and Pozzer, A.: The contribution of outdoor air pollution
469 sources to premature mortality on a global scale, *Nature*, 525, 367-371, 2015.
- 470 Lin, J. T., Youn, D., Liang, X. Z., and Wuebbles, D. J.: Global model simulation of summertime US ozone diurnal
471 cycle and its sensitivity to PBL mixing, spatial resolution, and emissions, *Atmospheric Environment*, 42,
472 8470-8483, 10.1016/j.atmosenv.2008.08.012, 2008.
- 473 Lin, M., Fiore, A. M., Horowitz, L. W., Langford, A. O., Oltmans, S. J., Tarasick, D., and Rieder, H. E.: Climate
474 variability modulates western US ozone air quality in spring via deep stratospheric intrusions, *Nature*
475 *Communications*, 6, 7105, 10.1038/ncomms8105, 2015.
- 476 Lin, M. Y., Horowitz, L. W., Payton, R., Fiore, A. M., and Tonnesen, G.: US surface ozone trends and extremes
477 from 1980 to 2014: quantifying the roles of rising Asian emissions, domestic controls, wildfires, and
478 climate, *Atmospheric Chemistry and Physics*, 17, 2943-2970, 10.5194/acp-17-2943-2017, 2017.
- 479 F. Meleux, F. Solmon, F. Giorgi: Increase in summer European ozone amounts due to climate change. *Atmospheric*
480 *Environment*, 41, pp. 7577-7587, 2007.
- 481 Monks, P. S., Archibald, A. T., Colette, A., Cooper, O., Coyle, M., Derwent, R., Fowler, D., Granier, C., Law, K. S.,
482 Mills, G. E., Stevenson, D. S., Tarasova, O., Thouret, V., von Schneidmesser, E., Sommariva, R., Wild, O.,
483 and Williams, M. L.: Tropospheric ozone and its precursors from the urban to the global scale from air
484 quality to short-lived climate forcer, *Atmospheric Chemistry and Physics*, 15, 8889-8973, 10.5194/acp-15-
485 8889-2015, 2015.
- 486 Pozzer, A., Jockel, P., Tost, H., Sander, R., Ganzeveld, L., Kerkweg, A., and Lelieveld, J.: Simulating organic
487 species with the global atmospheric chemistry general circulation model ECHAM5/MESSy1: a comparison
488 of model results with observations, *Atmospheric Chemistry and Physics*, 7, 2527-2550, 2007.

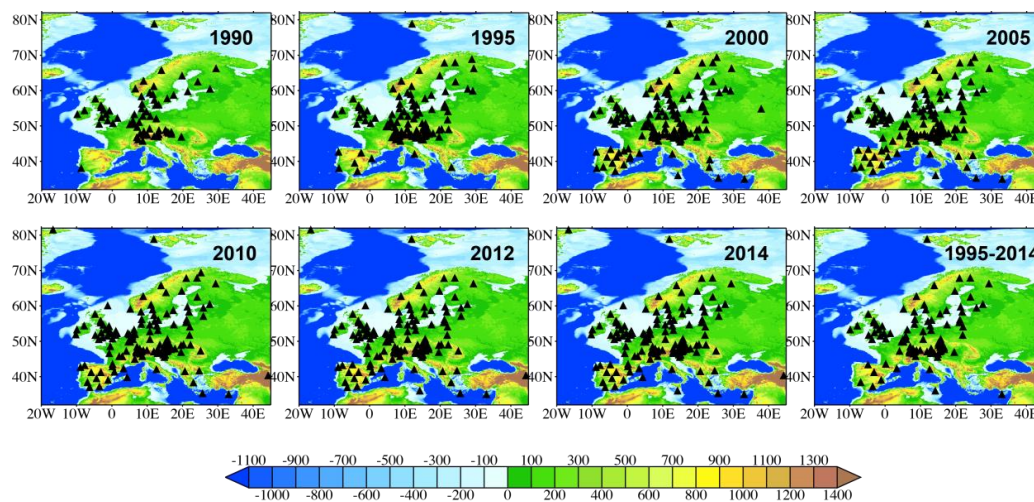


- 489 Pozzer, A., de Meij, A., Pringle, K. J., Tost, H., Doering, U. M., van Aardenne, J., and Lelieveld, J.: Distributions
490 and regional budgets of aerosols and their precursors simulated with the EMAC chemistry-climate model,
491 Atmospheric Chemistry and Physics, 12, 961-987, 10.5194/acp-12-961-2012, 2012.
- 492 Richter, A., Burrows, J. P., Nüss, H., Granier, C., and Niemeier, U.: Increase in tropospheric nitrogen dioxide over
493 China observed from space., Nature, 437, 129-132, 2005.
- 494 Roeckner, E., Brokopf, R., Esch, M., Giorgetta, M., Hagemann, S., Kornblueh, L., Manzini, E., Schlese, U., and
495 Schulzweida, U.: Sensitivity of simulated climate to horizontal and vertical resolution in the ECHAM5
496 atmosphere model, Journal of Climate, 19, 3771-3791, 10.1175/jcli3824.1, 2006.
- 497 Simon, H., Reff, A., Wells, B., Jia, X., and Frank, N.: Ozone Trends Across the United States over a Period of
498 Decreasing NO_x and VOC Emissions, Environmental Science & Technology, 49, 186-195, 2015.
- 499 Strode, S. A., Rodriguez, J. M., Logan, J. A., Cooper, O. R., Witte, J. C., Lamsal, L. N., Damon, M., Van Aartsen, B.,
500 Steenrod, S. D., and Strahan, S. E.: Trends and variability in surface ozone over the United States, Journal
501 of Geophysical Research-Atmospheres, 120, 9020-9042, 10.1002/2014jd022784, 2015.
- 502 Weatherhead, E. C., Reinsel, G. C., Tiao, G. C., Meng, X. L., Choi, D. S., Cheang, W. K., Keller, T., DeLuisi, J.,
503 Wuebbles, D. J., Kerr, J. B., Miller, A. J., Oltmans, S. J., and Frederick, J. E.: Factors affecting the detection
504 of trends: Statistical considerations and applications to environmental data, Journal of Geophysical
505 Research-Atmospheres, 103, 17149-17161, 10.1029/98jd00995, 1998.
- 506 Wilson, R. C., Fleming, Z. L., Monks, P. S., Clain, G., Henne, S., Konovalov, I. B., Szopa, S., and Menut, L.: Have
507 primary emission reduction measures reduced ozone across Europe? An analysis of European rural
508 background ozone trends 1996-2005, Atmospheric Chemistry and Physics, 12, 437-454, 10.5194/acp-12-
509 437-2012, 2012.
- 510 Yan, Y. Y., Lin, J. T., and He, C. L.: Ozone trends over the United States at different times of day, Atmos. Chem.
511 Phys. Discuss., 2017, 1-33, doi:10.5194/acp-2017-659, 2017
- 512 Yan, Y., Lin, J., Chen, J., and Hu, L.: Improved simulation of tropospheric ozone by a global-multi-regional two-
513 way coupling model system, Atmospheric Chemistry and Physics, 16, 2381-2400, 10.5194/acp-16-2381-
514 2016, 2016.
- 515 Yan, Y. Y., Lin, J. T., Kuang, Y., Yang, D., and Zhang, L.: Tropospheric carbon monoxide over the Pacific during
516 HIPPO: two-way coupled simulation of GEOS-Chem and its multiple nested models, Atmospheric
517 Chemistry and Physics, 14, 12649-12663, 10.5194/acp-14-12649-2014, 2014.
- 518 Yoon, J., and Pozzer, A.: Model-simulated trend of surface carbon monoxide for the 2001-2010 decade, Atmospheric
519 Chemistry and Physics, 14, 10465-10482, 10.5194/acp-14-10465-2014, 2014.
- 520 Dee, D. P., and Uppala, S.: Variational bias correction of satellite radiance data in the ERA-Interim reanalysis,
521 Quarterly Journal of the Royal Meteorological Society, 135, 1830-1841, 10.1002/qj.493, 2009.
522
523
524
525



526

527



528

529

530

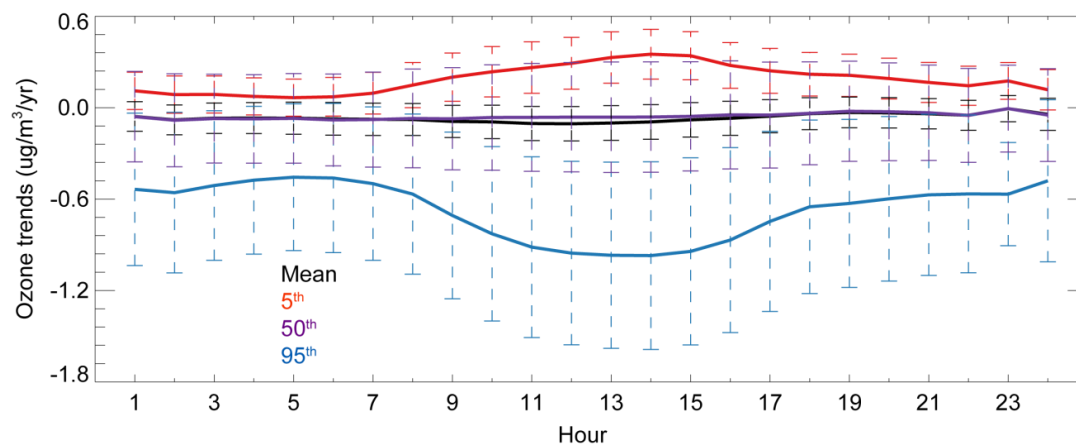
531

532

Fig. 1. Site distribution for the EMEP datasets (1990-2014) as well as the selected 93 sites (1995-2014). The overlaid map shows the surface elevation (m) from a 2 min Gridded Global Relief Data (ETOPO2v2) available at NGDC Marine Trackline Geophysical database (<http://www.ngdc.noaa.gov/mgg/global/etopo2.html>).



533



534

535

536

537

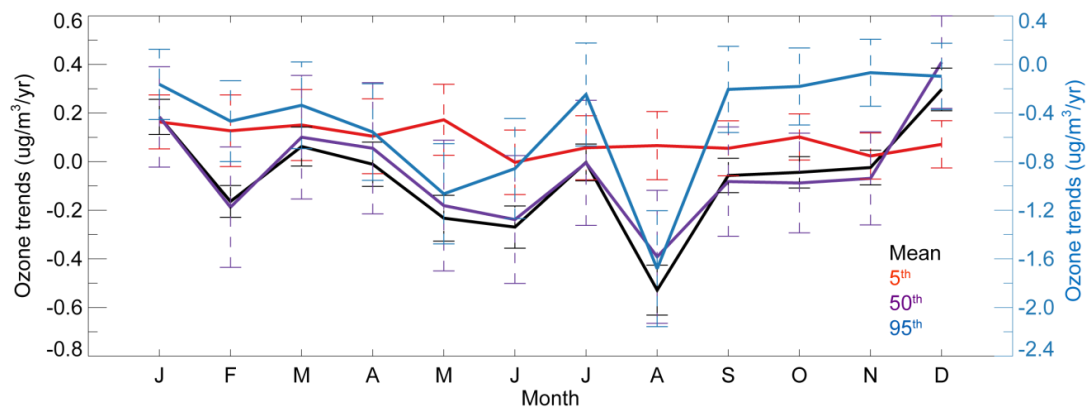
538

539

Fig. 2. Trend in the observed surface ozone averaged over Europe, calculated for the selected 93 sites. The black line shows the 1995–2014 linear trends in the deseasonalized European monthly ozone anomalies for each hour of the day (local standard time), the red, purple and blue lines depict the observed trend for 5th, 50th and 95th percentile ozone, respectively, and the dashed bars indicate their standard deviations.



540



541

542

543

544

545

546

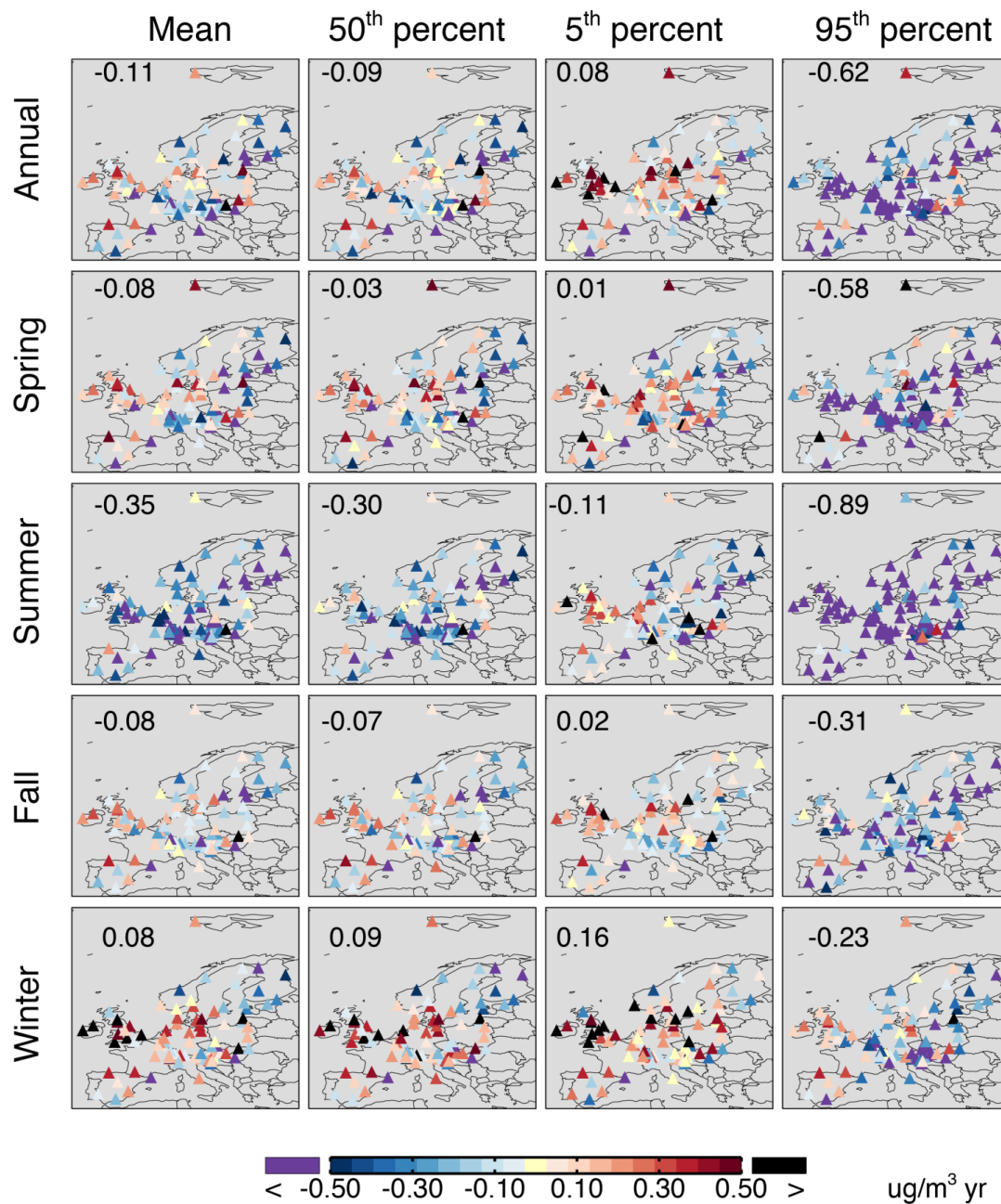
547

548

Fig. 3. Monthly trend in the observed surface ozone averaged over Europe for the selected 93 sites. The black line shows the 1995–2014 linear trends in the European mean ozone for each month of the year, the red, purple and blue lines depict the observed trend for 5th, 50th and 95th percentile ozone, respectively, and the dashed bars indicate their standard deviations. The left axis is for the trends of mean, 5th, and 50th percentile ozone, while the right axis for the 95th percentile ozone.



549



550

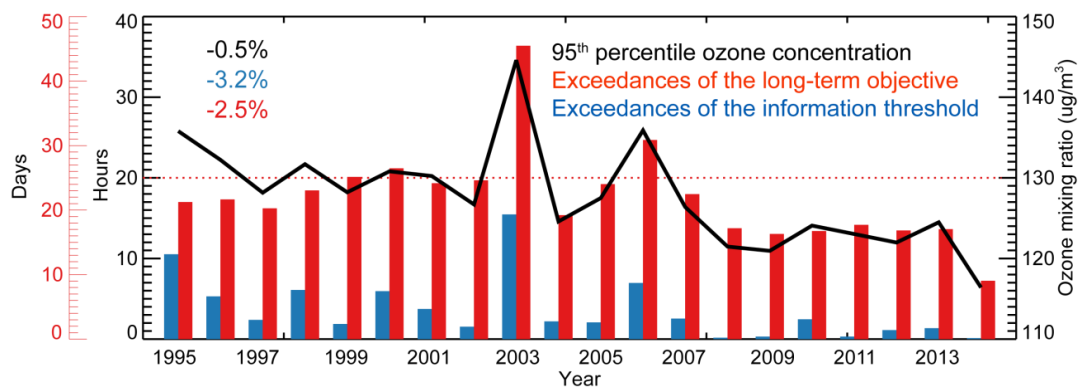
551

552

553

554

Fig. 4. Spatial distribution of measured daytime ozone trends in $\mu\text{g}/\text{m}^3$ across the selected 93 sites for average, 5th, 50th and 95th percentile ozone in annual mean and four seasons. Also shown in each panel are the average trends over all sites.



555

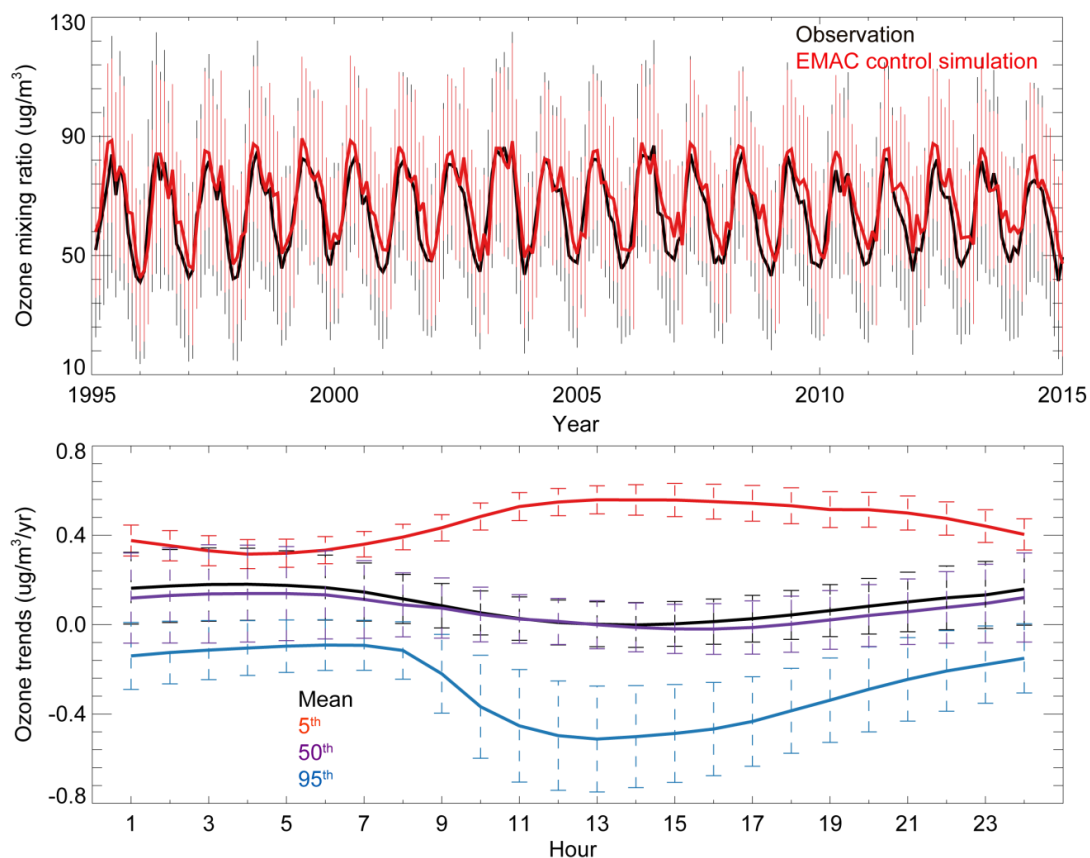
556

557 Fig. 5. Annual exceedances of the information threshold (for blue bars, hours should be multiplied by 100, 1-hourly

558 averages: $180 \mu\text{g}/\text{m}^3$) as well as the long-term objective (red bars, maximum diurnal 8-hourly mean: $120 \mu\text{g}/\text{m}^3$),

559 compared with the annual 95th percentile ozone concentrations (black line). Red dotted line shows the target value

560 (long-term objective that should not be exceeded more than 25 days per year, averaged over 3 years).



561

562 Fig. 6. EMAC modeled ozone in $\mu\text{g}/\text{m}^3$ over Europe during 1995-2014. Time series of measured (black) and

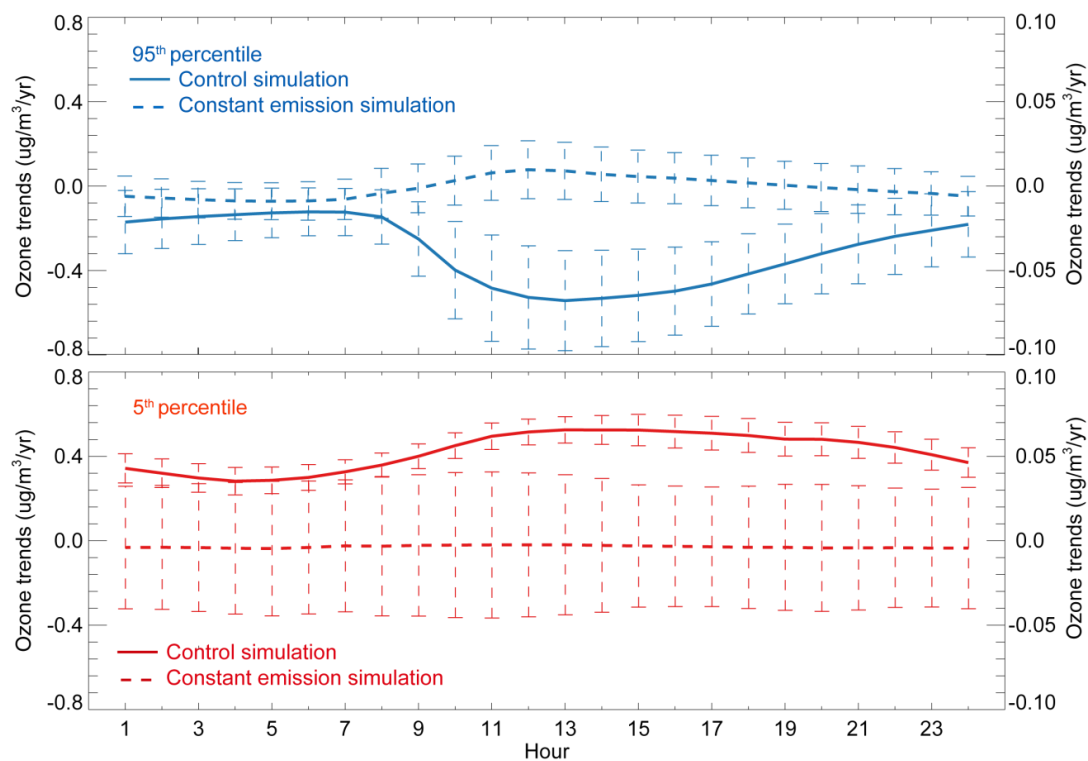
563 modeled (red) monthly mean ozone over the 93 selected sites (top). Trend in the modeled surface ozone averaged

564 over the selected 93 sites for all hours of the day (local time, bottom). The black line shows the 1995-2014 linear

565 trends in the European mean ozone, the red, purple, and blue lines are the modeled trends for 5th, 50th and 95th

566 percentile ozone, respectively. The dashed bars indicate their standard deviations.

567



568

569

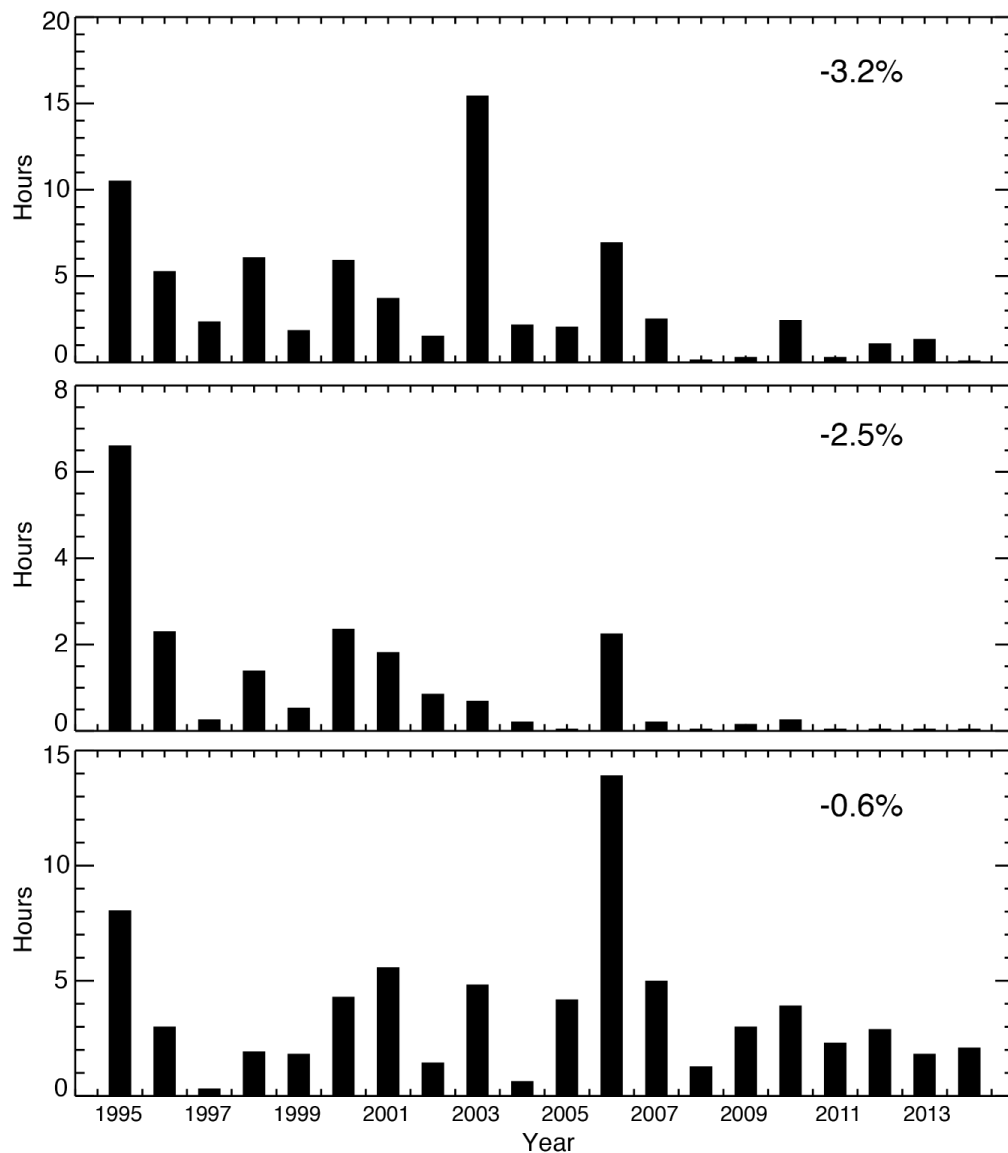
570 Fig. 7. Modeled trend in the surface ozone averaged over the selected 93 sites for all hours of the day (local time).
571 The solid lines (left legends) show the 1995-2014 linear trends in the control simulation for 95th (top) and 5th
572 percentile (bottom) ozone, respectively. The dashed lines (right legends) represent the modeled trends by the
573 constant emission simulation. The bars indicate their deviations.

573

574



575



576

577

578

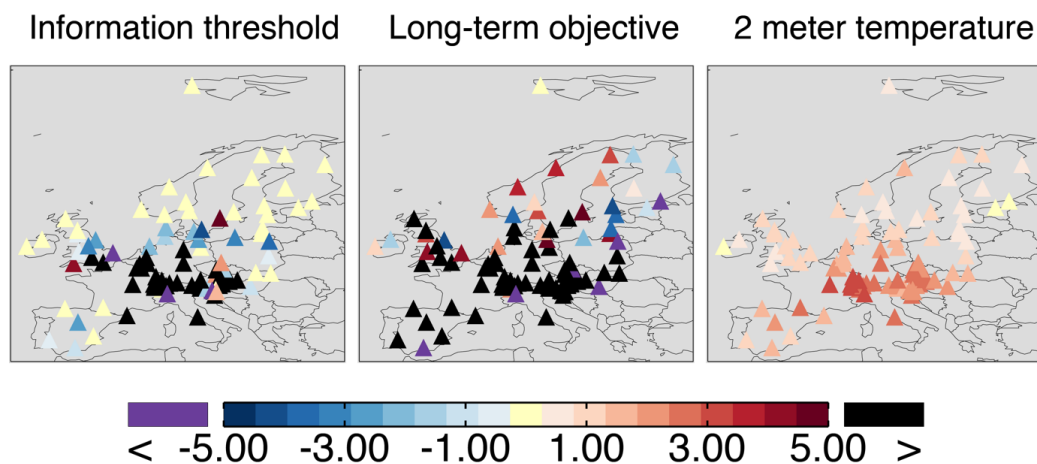
579

580

Fig. 8. Annual observed (top) and modeled (middle: control simulation; bottom: constant emission simulation) exceedances of the information threshold (1-hourly averages: 180 µg/m³). The hours along the y-axis should be multiplied by 100.



581



582

583 Fig. 9. Spatial distribution of the exceedance anomalies in 2003, relevant to the averages over 1995-2002 and for the
584 information threshold as well as the long-term objective, in comparison with the 2-meter temperature anomalies in
585 each of the sites.
586



587 Table 1. Percentage of missing hourly data in each year.

Year	Number of sites	Missing data		
		Whole day	Daytime	Nighttime
1995	113	32.6%	30.6%	34.6%
1996	115	28.8%	26.7%	30.9%
1997	121	23.9%	21.6%	26.2%
1998	120	18.5%	16.0%	21.0%
1999	127	10.4%	7.9%	12.8%
2000	132	9.8%	7.2%	12.3%
2001	134	11.9%	9.4%	14.4%
2002	136	9.3%	6.8%	11.8%
2003	137	12.1%	9.8%	14.4%
2004	135	10.9%	8.5%	13.3%
2005	132	10.5%	8.1%	12.9%
2006	130	10.6%	8.1%	13.1%
2007	132	9.5%	7.0%	12.0%
2008	136	10.8%	8.2%	13.4%
2009	134	10.6%	7.8%	13.3%
2010	136	15.0%	12.6%	17.5%
2011	135	13.8%	11.4%	16.2%
2012	136	14.1%	11.8%	16.4%
2013	136	19.9%	17.8%	22.0%
2014	137	21.0%	19.1%	23.0%

588

589



590 Table 2. Modeled and observed ozone trends and their standard deviations based on diurnal
591 average ozone concentrations. The mean, 5th, 50th, and 95th percentile represent the monthly
592 statistics of the diurnal averages. The model has been sampled in the same location of the EMEP
593 stations.

	5 th percentile	50 th percentile	Mean	95 th percentile
EMEP ($\mu\text{g}/\text{m}^3/\text{y}$)	0.22 ± 0.15	-0.05 ± 0.23	-0.07 ± 0.21	-0.57 ± 0.34
EMAC ($\mu\text{g}/\text{m}^3/\text{y}$)	0.42 ± 0.14	0.01 ± 0.10	0.06 ± 0.09	-0.23 ± 0.10

594

595



596

597 Table 3. Modeled and observed linear trends and their standard deviations of the 1995–2014
598 European mean annual and seasonal averaged daytime and nighttime mean as well as their 5th,
599 50th and 95th percentile ozone concentrations.

600

	Seasons	Mean		5 th percentile		50 th percentile		95 th percentile	
		EMEP	EMAC	EMEP	EMAC	EMMP	EMAC	EMEP	EMAC
Daytime ($\mu\text{g}/\text{m}^3/\text{y}$)	Annual	-0.09 ± 0.24	0.00 ± 0.06	0.22 ± 0.17	0.45 ± 0.14	-0.06 ± 0.24	-0.01 ± 0.06	-0.81 ± 0.46	-0.48 ± 0.15
	MAM	-0.09 ± 0.27	-0.05 ± 0.08	0.13 ± 0.24	0.52 ± 0.17	-0.02 ± 0.27	-0.02 ± 0.08	-0.93 ± 0.53	-0.49 ± 0.16
	JJA	-0.32 ± 0.24	-0.10 ± 0.07	-0.03 ± 0.26	0.41 ± 0.20	-0.26 ± 0.24	-0.09 ± 0.13	-1.10 ± 0.61	-0.54 ± 0.16
	SON	-0.03 ± 0.19	-0.04 ± 0.05	0.09 ± 0.14	0.36 ± 0.12	-0.04 ± 0.20	-0.02 ± 0.05	-0.24 ± 0.25	-0.44 ± 0.23
	DJF	0.10 ± 0.25	0.18 ± 0.14	0.25 ± 0.15	0.39 ± 0.22	0.05 ± 0.27	0.15 ± 0.20	-0.28 ± 0.31	-0.08 ± 0.05
Nighttime ($\mu\text{g}/\text{m}^3/\text{y}$)	Annual	-0.05 ± 0.23	0.12 ± 0.11	0.16 ± 0.17	0.38 ± 0.19	-0.05 ± 0.24	0.07 ± 0.12	-0.57 ± 0.36	-0.21 ± 0.10
	MAM	-0.06 ± 0.29	0.08 ± 0.10	0.18 ± 0.23	0.23 ± 0.23	-0.00 ± 0.29	0.04 ± 0.08	-0.64 ± 0.43	-0.20 ± 0.12
	JJA	-0.20 ± 0.27	0.06 ± 0.14	0.07 ± 0.24	0.36 ± 0.22	-0.15 ± 0.28	0.04 ± 0.14	-0.71 ± 0.52	-0.36 ± 0.21
	SON	-0.03 ± 0.21	0.06 ± 0.10	0.05 ± 0.12	0.19 ± 0.16	-0.05 ± 0.23	0.04 ± 0.11	-0.21 ± 0.24	-0.23 ± 0.19
	DJF	0.09 ± 0.24	0.24 ± 0.18	0.14 ± 0.22	0.43 ± 0.27	0.06 ± 0.25	0.20 ± 0.25	-0.24 ± 0.29	-0.05 ± 0.06

601